High pressure kinetics of CH$_4$, CO and H$_2$ combustion over LaMnO$_3$ catalyst

Gianluca Landi [a], Paola Sabrina Barbato [a,b,*], Almerinda Di Benedetto [b], Raffaele Pirone [c], Gennaro Russo [b]

[a] Research Institute on Combustion-CNR, Naples, Italy
[b] Dep. of Chem. Eng., Univ. of Naples Federico II, Naples, Italy
[c] DISAT, Politecnico di Torino, Turin, Italy

ARTICLE INFO

ABSTRACT

A high pressure kinetic study was carried out in a wide range of operating conditions to study the effects of pressure, temperature, fuel concentration and equivalence ratio on the catalytic combustion of methane, hydrogen and carbon monoxide over a perovskite-based catalyst. A plate type reactor configuration was chosen. This geometry allowed working in a kinetic control avoiding mass transfer limitations if appropriate experimental conditions are chosen. Since especially for GT application it is important to study the ignition phenomenon, which results to be ruled by kinetics, the study of the kinetics of CH$_4$, H$_2$ and CO catalytic combustion was carried out in a range of temperature consistent with the ignition temperatures and global reaction rate equations were derived.

© 2013 Elsevier B.V. All rights reserved.

1. Introduction

Catalytic combustion allows converting light hydrocarbons at relatively low temperatures and with very high combustion efficiency, thus avoiding NO$_x$ formation and CO and HC emissions. It is then considered an alternative route to produce power with low environmental impact [1] and then suitable for gas turbine (GT) applications. In particular, it has been demonstrated that catalytic combustion is very attractive where ultra-low NO$_x$ levels are required and for small size GT, for which secondary measures turn out to be very expensive [2].

Recently a great attention has been devoted to the study of the combustion not only of methane but also of fuel mixtures containing hydrogen and/or carbon monoxide at gas turbine conditions relevant for power generation both under homogeneous [3] and heterogeneous (catalyzed) reaction conditions [4,5]. Mixtures containing H$_2$/CO, derived from gasification of solid or liquid fuels as it occurs in IGCC plants and eventually added with NG, are used as fuel in GT combustors. However, the partial or total replacement of methane with these low calorific value fuels is usually accompanied by an increase of adiabatic temperature and then NO$_x$ production even for established technologies such as gas turbines. In this

scenario the catalytic option is a valid alternative to the homogeneous one also taking into account that H$_2$ and CO, with the choice of the appropriate catalytic system, are easily converted also at very low temperatures thus improving the CH$_4$ combustion [6].

The most active catalysts are based on noble metals [7,8]; they are generally used for VOC abatement at low and medium temperature as it occurs in three way catalysts. The major drawback is related to their cost and tendency to volatilize and/or sinter at high temperature [9].

Amongst different types of metal oxides, perovskites (general formula ABO$_3$) have been extensively proposed as total oxidation catalysts [8]. Moreover the structure robustness permits the partial substitution of A and B cations with metals with a different oxidation state ($A_xA'_{1-x}B_yB'_{1-y}O_{3-\delta}$). The partial substitution results into the profound modification of the activity since it leads to the formation of structural defects promoting catalytic activity of the material [10].

Formulations in which A sites are occupied by La or La–Sr and B sites are occupied by Co, Fe, o Mn [11] are the most active phases for methane combustion, Mn-based perovskite showing the best performance [12]. However, the application of perovskites is limited by their low surface area and at temperatures above 800 °C sintering of perovskite-oxides occurs caused by the 3D growth of crystals. In order to overcome these problems, the active phases have been dispersed over high surface area supports such as La-stabilized alumina or La-stabilized MgO or spinels with a resulting increase of activity and thermal stability [13,14]. To increase the perovskite

Nomenclature

Symbols

a	Gas–solid interfacial area per mass of catalyst in Eq. (7)
C, C°	Molar concentration, initial fuel molar concentration (mol l^{-1})
C_s	External surface concentration of reactant (mol l^{-1})
D_e	Dispersion coefficient
$\mathfrak{D}_{eff}$	Effective diffusion in pores (m^2 s^{-1})
$\mathfrak{D}_M, \mathfrak{D}_{M,eff}$	Molecular or ordinary diffusivity, ordinary effective diffusion (m^2 s^{-1})
$\mathfrak{D}_K, \mathfrak{D}_{K,eff}$	Knudsen diffusion, effective diffusivity (m^2 s^{-1})
F	Ratio of the model mean square to the error mean square
N_{obs}, N_{para}	Number of experimental observation and number of model parameter
k, k_i	Kinetic constants
K, K_i	Adsorption constants (bar^{-1})
$\widehat{k}_g$	Mass transfer coefficient (kmol(m^2 s)$^{-1}$)
K_m	Mass transfer coefficient (kmol(m^2 s bar)$^{-1}$)
L	Reactor length (m)
M	Molecular weight (g mol^{-1})
Mrss	Mean residual sum of squares
P, P_i	Total pressure, partial pressure of the i specie
P_s, P_b	Fuel partial pressure on the surface, in the gas bulk
Q_{TOT}	Total volumetric flowrate (slph)
r, r_i	Rate of fuel consumption (mol(g s)$^{-1}$)
R	Ideal gas constant (l atm K^{-1} mol^{-1})
S	Outer catalytic surface per unit of weigth (m^2 g^{-1})
SSA	Specific surface area (m^2 g^{-1})
u	Gas velocity (m s^{-1})
W	Width (m)
$x_{p,n}, x_n$	Predicted and experimental final conversion for the nth experiment
y_i, y_i°	Molar fraction of i specie, initial molar fraction of i specie
z	Reactor axial coordinate

Subscripts used for kinetic and adsorption constants in models 1–22

c	Carbon monoxide
h	Hydrogen
m	Methane
o	Oxygen

Greek symbols

δ	Height of the combustion chamber (m)
δ_H	Hydraulic diameter of the reactor (m)
δ_{cat}	Thickness of catalytic layer (m)
η	Efficiency factor
θ, τ	Void fraction and tortuosity factor in Eqs. (11) and (12)
μ	Gas viscosity
ρ	Gas density
τ	Contact time (g s l^{-1})
φ_l	Thiele modulus
Φ	Weisz modulus

Non dimensional groups

Re	(Reynolds number) $\rho u \delta_H / \mu$
Sc	(Schmidt number) $\mu / (\rho \mathfrak{D}_M)$
Sh	(Sherwood) $(\widehat{k}_g R T \delta_H / \mathfrak{D}_M P)$
Pe$_{ax}$	(axial Peclet) uL/D_e

activity, bi-functional catalysts have been developed by doping the perovskite with small amounts of noble metals [15–19]. Up to now, this catalyst represents the best compromise combining high reactivity at low temperature and stable operation at relatively high temperature.

A high number of papers have been devoted to the study of catalytic combustion at atmospheric pressure. However, the relative weight of the phenomena involved in catalytic combustion may be significantly affected by the working pressure [20–27]. As a consequence, *it is not unusual to hear of catalysts that appear to have worked well in a laboratory environment but do not so when installed in a High Pressure pilot-scale rig"* [28].

Generally, detailed reaction schemes for the catalytic combustion of methane over noble metal catalysts [29–31] have been validated also at high pressure [23,25]. Moreover, Mantzaras and co-workers performed experimental and numerical studies on syngas combustion over Pt-based catalysts, simulations being based on a detailed kinetic scheme [32].

However, for engineering purposes, global reaction rate equations must be derived. Snow et al. [33] derived a global reaction rate for methane combustion over Pt, finding a reaction order with respect to total pressure equal to 0.4.

Reinke et al. [23] investigated the catalytic combustion of CH$_4$/air over Pt at pressures up to 16 bar, eventually deriving a global reaction rate taking into account the effect of total pressure. They found that the reaction rate depends on pressure by a factor of 0.5, suggesting a sort of inhibition effect of pressure on the combustion kinetics.

According to the above considerations, it appears that the study of the combustion of H$_2$/CO/CH$_4$ mixtures over non-noble metal catalyst is of great interest. Nevertheless, there is a lack of knowledge about the combustion kinetics of these fuels on perovskite catalysts under operating conditions typical of gas turbines.

In this work we perform a preliminary kinetic study of the catalytic combustion of methane, carbon monoxide and hydrogen over a LaMnO$_3$ catalyst, at pressure up to 10 bar. In a future work we will report the kinetic behavior of the H$_2$/CO/CH$_4$ mixtures.

We performed the experiments over a supported LaMnO$_3$ catalyst in a plate type structured reactor. This structured reactor allows: (i) the easiness of catalyst loading control obtained choosing the thickness and length of the catalyst layer; (ii) the laminar regime conserved in a wide range of flow rates, thus limiting pressure drops, (iii) the resemblance with structured catalyst usually used for industrial application and (iv) the well-defined geometry that makes mathematical modeling effective for design purposes [34–37]. We tested several reaction rate equations and finally we derived the best kinetic equation for CH$_4$, CO and H$_2$ combustion.

2. Experimental

2.1. Catalyst preparation and characterization

Structured catalysts in form of platelets have been prepared according to the procedure reported in [19]. Powder catalysts have been preliminary prepared by supporting the active phase on finely grounded γ-Al$_2$O$_3$ (AKZO CK 300), previously stabilized by inserting lanthanum oxide (5 wt%) into the structure in order to avoid γ-to α-alumina transition [38].

The active phase and La$_2$O$_3$ are deposited through an "incipient wetness impregnation" method in a rotary vapour (Laborota 4002, Heidolph) by suspending the inert alumina powder in an aqueous solution constituted by active phase precursors (manganese acetate tetrahydrate (Aldrich) and lanthanum nitrate hexahydrate

Fig. 1. LM20 platelet.

Table 1
Reactor geometrical properties.

Platelet	
W, width	0.015 m
L, length	0.03 m
δ_{cat}, catalytic layer thickness	0.000045 m
S, outer catalytic surface per unit of weight	0.0017 m^2 g^{-1}
Combustion chamber	
δ, channel gap	0.001 m
Hydraulic diameter $\delta_H = 4\frac{W\delta}{2(W+\delta)}$	0.0018 m

(Fluka)). The dried impregnated powder is subsequently calcined at 800 °C for 3 h in air.

Alumina platelets (0.5 cm thick, 1.5 cm wide, 3.0 cm long) characterized by an elevated thermal, mechanical and chemical resistance have been prepared starting from precursors supplied by Cotronics. According to the recipe supplied by Cotronics [39], a specific amount of alumina powder (Rescor 780) and liquid activator (Rescor 780 Activator) are mixed in a beaker until obtaining a slurry provided with a certain consistency. The slurry is then poured in a home-made flexible and impermeable mold and dried at room temperature for about 20 h. Then the platelet is removed from the mold and the sample is further heated up to 950 °C (1 °C/min) for 5 h in order to further increase the mechanical resistance and to remove the organic part present in the liquid activator.

Finally, in order to deposit the catalytic film on the alumina substrates, a slurry constituted by the fresh powder catalyst is prepared. Powder is mixed with Boehmite (Disperal, Sasol), used as binder. The solid mixture is thus suspended in HNO$_3$ aqueous solution. The slurry is spread on the plate through a paintbrush and the excess was blown-out and, subsequently, the platelet is dried at 120 °C for 20 min. Finally, a calcination at 800 °C for 3 h is carried out in order to anchor the catalytic film on the substrate. The slurry deposition is repeated until a catalyst load of 20–30 mg was obtained. A catalytic layer thickness of about 50 μm was estimated by SEM analysis (Philips XL30 instrument). Onto the final structured catalyst, named LM20, 26 mg active layer was deposited; the perovskite content was 20 wt% with respect to the active layer. A picture of the so prepared catalyst is reported in Fig. 1.

Chemical composition of the active layer has been measured by means of inductively coupled plasma (ICP) analysis, performed on an Agilent 7500 ICP-MS instrument, while the adhesion of the active layer has been tested by ultrasound treatment (30 min) in a ultrasonic bath (Quantex 90H, L&R Manufacturing) in order to evaluate the resistance to mechanical stresses. ICP analysis revealed that catalyst composition is very close to the theoretical one. No significant weight difference between so prepared and ultrasound-treated

sample has been measured, suggesting that high mechanically resistant structured catalyst can be prepared by the preparation method described above.

2.2. High pressure reactor

As previously reported [19], the kinetic data were collected by using a plate-type reactor made in stainless steel and sketched in Fig. 2.

In a high temperature stainless steel (AISI 310S) cylinder (external diameter 25.4 mm, length 50 mm) three cavities have been obtained covering the overall cylinder length. In the middle there is a high precision rectangular chamber 6 mm high, 15 mm wide and 30 mm long. In this way, when the platelet is inserted, a 1 mm gap is determined above the platelet thus creating the combustion chamber (see Table 1).

At the two edges of the rectangular chamber, two circular housing (d = 17 mm; l = 10 mm) have been obtained and used for the allocation of SiC foams (45 ppi) in order to well distribute the mass flow of the gas in correspondence to the inlet and the outlet of the catalyst and, at the same time, to block the platelet in the appropriate position. Moreover there are two dead end circular holes (d < 1.5 mm) 1 mm above and below the rectangular chamber for thermocouples insertion. In this way the thermal profile along the axial direction and the temperature difference between upside and downside (i.e. below the platelet) wall of the chamber are detected limiting thermocouples contribution to the reaction and without altering the flow pattern in the combustion chamber. 1 in. A-lock fittings were used for gas connections providing a sealing up to 12 bar. Moreover, 4 thermocouples were sealed thanks to a Multiple-Hole Ceramic gland (Conax Buffalo, MHC series).

2.3. Test rig under pressure and experimental conditions

The lab-scale set-up, designed to work at pressures up to 12 bar, has been home-made and can be ideally divided into three sections: gas feed preparation and control, reaction zone and analysis.
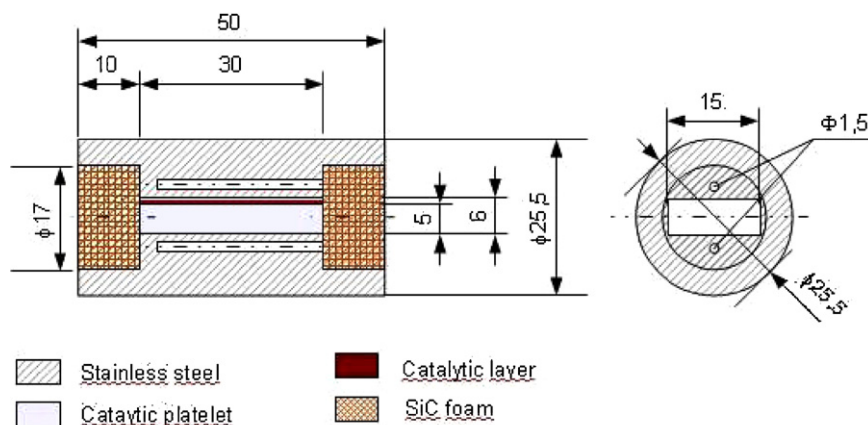

Fig. 2. Schematic representation of the stainless steel reactor.

The latter is at atmospheric pressure. O_2, N_2, CH_4, H_2 and CO from gas cylinders at high purity (CH_4: 99.995%; O_2: 99.7%; N_2: 99.998%) or as certified mixtures ($15\%H_2/N_2$; $5\%CO/N_2$) have been indipendently controlled through mass flow controllers (Brooks SLA5850S), operating at 15 bar and each one having downstream their own two-way electrovalve operated by remote control in order (i) to block the gas flow of unused gasses and, (ii) to interupt the flow of all gasses in case of danger. Besides, a pressure transducer (ABB 261G) is placed just downstream the gasses mixing point thus allowing the on-line monitoring of the pressure in the first section of the rig. A system of three two-way remote-controlled electrovalves simulates a four-way valve allowing the analysis of both reacting mixture and reactor off products. A second pressure transducer (ABB 261G) is positioned just upstream the reactor thus allowing the pressure measure at the reactor inlet also when the reactor is bypassed.

An heating jacket (Tyco Thermal Controls) equipped with a PID controller provides for the external heating of the reactor at the desired temperature. In order to avoid indesired water condensation, especially at high pressure, the reactor exit line was maintained at 120 °C till the entrance of a condenser (Parker). Finally, the dry gasses or the reacting mixture, on dependence of "four way" valve position, flow through the pressure controller (Brooks SLA5820), which regulates the upstream pressure in the range 0–15 bar gauge regardless of the total gas flow rate. The remainder of the plant is, then, at a pressure slightly above the atmospheric one. A constant fraction of the gas flow rate is further dried by means of a $CaCl_2$ chemical trap before entering into the analysis system (ABB AO2000), provided with five equipments for the on-line and continous analysis of the main gas species (CH_4, CO_2 and CO by infrared detectors, O_2 by paramagnetic detector and H_2 by a thermoconducibility detector) and equipped with a cross sensitivity correction.

Diluted CH_4, H_2 and CO mixtures were used for the assessment of the more appropriate kinetic law and the temperature dependence of the kinetic parameters. We used low fuel concentrations in order to avoid thermal gradients along the reactor. The catalyst was previously aged in air at 800 °C for at least 12 h, thus providing stable performance [16]. In Table 3, the operative conditions adopted for the combustion tests under pressure are summarized. In particular, the temperature ranges have been chosen to be consistent with those used during the ignition, which is ruled by kinetics. As a matter of fact, at high temperature mass transfer limitation and homogeneous reaction occurrence limit the role of surface kinetics [19,22].

2.4. Reactor model and numerical methodologies

Different reaction rates have been tested in order to find the best model representing the combustion rates of CH_4, H_2 and CO over $LaMnO_3$ perovskite catalyst. The model discrimination was done using the criterion of the minimization of the mean residual sum of squares (Mrss) defined by the following expression:

$$\text{Mrss} = \sum_{n=1}^{N} \frac{(x_{p,n} - x_n)^2}{N_{\text{obs}} - N_{\text{para}}} \tag{1}$$

where the $x_{p,n}$ and x_p are respectively the predicted and experimental conversion of the nth experiment, N_{obs} is the number of experimental observation and N_{para} is the number of parameters used in the model. Among the models returning very low Mrss values those showing parameters with no physical meaning were rejected.

In order to express the experimental conversion functionality with respect to temperature, pressure, reactant molar fractions and contact time, it was necessary to develop an appropriate

Table 2
Operative conditions adopted for the tests under isothermal condition.

	CH_4	H_2	CO
Fuel, %	0.15–1	0.25–1	0.25–1
O_2, %	8.5	2–8.5	2–8.5
Q_{TOT}, slph	55–80	75	75
τ, gsl(STP)$^{-1}$	1.7–1.2	1.25	1.25
GHSV (h^{-1})	1.2×10^5 to 1.8×10^5	1.7×10^5	1.7×10^5
Temperature range, °C	555–620	470–530	470–530

reactor model. Accordingly, the reactor was assimilated to a Plug Flow Reactor (PFR) with negligible mass transfer limitation; this assumption has been preliminarily verified (see Section 3). As a consequence, the reactor constitutive equation relating conversion and contact time is:

$$\int_0^{x_{fin}} \frac{dx}{r} = \frac{\tau}{C^0} = \frac{RT\tau}{Py^0} \tag{2}$$

By means of Eq. (2), the final conversion is related to the above mentioned variables (temperature, pressure, contact time and so on) and, after expressing r, also to kinetic parameters. Eq. (2) relates the intrinsic catalytic reaction rate to measurable parameters in the overall range of conversion provided that the impact of mass transfer limitation is not significant.

Therefore the model parameters have been identified by fitting the experimental observed final conversions with the implicit functionality expressed in Eq. (2). Nonlinear fitting has been performed by a least-squares fitting algorithm implemented in the *nlinfit* function of Matlab (Mathworks®) [40] obtaining, other than the evaluated parameters, several statistical output data, such as Mrss, confidence intervals and *F*-test values.

In addition, due to the strong correlation between activation energies and pre-exponential factor, the following reparameterization was adopted for kinetic constant (Eq. (3)) and for adsorption constant too (Eq. (4)).

$$k_i = k_{i0} \exp\left(-\frac{E_{ai}}{R}\left(\frac{1}{T} - \frac{1}{T_m}\right)\right) \tag{3}$$

$$K_i = K_{i0} \exp\left(-\frac{\Delta H_i}{R}\left(\frac{1}{T} - \frac{1}{T_m}\right)\right) \tag{4}$$

3. Preliminary results

3.1. Plug flow approximation

First an evaluation of the magnitude of axial Peclet number (Pe_{ax}) defined as follows

$$\text{Pe}_{\text{ax}} = \frac{uL}{D_e},$$

was done in order to mark off the operative conditions for which the plug flow hypothesis is valid. According to Levenspiel the flow can be considered plug for Pe_{ax} higher than 30 [41]. The following empirical correlation for dispersion coefficient, valid for $1 < \text{Re} < 2000$ (i.e. for laminar flow) and $0.2 \leq \text{Sc} \leq 1000$ was used [42]:

$$\frac{D_e}{u\delta_H} = \frac{1}{\text{ReSc}} + \frac{\text{ReSc}}{192} \tag{5}$$

where the dimensionless group ReSc is pressure independent.

Our calculations (not reported) revealed that under the experimental conditions used in this work (see Table 2) Pe_{ax} is always higher than 30, thus suggesting that the flow can be considered plug.

Table 3
Literature kinetic parameters used for computing $k/(K_m a)$ and P_s/P_b ratios.

CH$_4$[a]		H$_2$[b]		CO[b]	
E_a, kcal mol^{-1}	$k°$, slph(g s)$^{-1}$	E_a, kcal mol^{-1}	$k°$, slph(g s)$^{-1}$	E_a, kcal mol^{-1}	$k°$, slph(g s)$^{-1}$
26.2	3.6×10^5	14.6	2.68×10^3	13.0	3.53×10^3

[a] From Scarpa et al. [17].
[b] From Cimino et al. [44].

3.2. Interphase limitation to mass transfer

The relative importance of interphase limitation to mass transfer of reactants from gas bulk to catalytic surface was evaluated by computing the following ratio:

$$\frac{k}{K_m a} = \frac{P_b - P_s}{P_s} \tag{6}$$

that expresses the ratio between surface reaction, considering a first order reaction, and diffusion characteristic times and quantifies the fuel concentration drop from gas bulk to catalytic surface. Accordingly, conditions returning a ratio much smaller than 1 are free from external diffusion control.

At this purpose mass transfer coefficient K_m has been evaluated from Sherwood number (Sh) according to Eq. (7).

$$\text{Sh} = \frac{\widehat{k_g} RT \delta_H}{\mathfrak{D}_M P} = \frac{K_m RT \delta_H}{\mathfrak{D}_M} \tag{7}$$

In order to make a conservative evaluation, Sh equal to 5.6 was considered. This value, corresponding to the limiting Sh value (Sh$_\infty$) in rectangular ducts with an aspect ratio equal to 8, underestimates the real Sh$_\infty$ value corresponding to the higher aspect ratio of the our combustion chamber equal to 15 [43]. Moreover taking into account the following expression for local Sh number [44]:

$$\text{Sh}_{loc} = \text{Sh}_\infty + 8.827 \left(\frac{1000z}{\delta_H ReSc} \right)^{-0.545} \exp \left(\frac{-48.2z}{\delta_H ReSc} \right) \tag{8}$$

it is evident that local Sh is even higher than its limiting value.

Concerning kinetic constants, their values have been estimated at different temperatures preliminary considering first order reaction with respect to the fuel from literature data, reported in Table 3.

According to our calculations (not reported), it clearly appears that in a wide range of temperatures P_s/P_b ratios are close to 1 for each fuel within their temperature range of interest. As a consequence, experiments reported in the following are unaffected by external transport limitations. It is worth noting that the above considerations are valid independently from the overall pressure and local concentrations. Calculations performed after obtaining the most suitable kinetic expressions returned similar results.

3.3. Intraphase limitation to mass transfer

The impact of intraphase transport limitation was considered according to the Weisz–Prater criterion (Eq. (9)) that allows to determine the importance of internal diffusion using all observable variables. Properly in the case of integral reactor the C_s or C_b have to be replaced by the proper average of the varying concentrations.

$$\Phi = \phi_L^2 \eta = \frac{\delta_{cat}^2 r_v}{C_s \mathfrak{D}_{eff}} < 0.3 \tag{9}$$

In the case of this preliminary study the Weisz modulus Φ has been calculated for the initial concentration. By increasing the pressure, not only the surface concentration of reactants is increased, but also the diffusion mechanism can be changed. The effective diffusivity has been calculated according to Eq. (10)

$$\frac{1}{\mathfrak{D}_{eff}} = \frac{1}{\mathfrak{D}_{K,eff}} + \frac{1}{\mathfrak{D}_{M,eff}} \tag{10}$$

i.e. taking into account both Knudsen and ordinary diffusion mechanisms.

Concerning the ordinary diffusion, the effective diffusion was estimated by the following equation (Eq. (11)):

$$\mathfrak{D}_{M,eff} = \mathfrak{D}_M \frac{\theta}{\tau} \tag{11}$$

where the τ factor takes into account for both tortuosity and pore cross section variation.

From Eq. (11) it appears that the $\mathfrak{D}_{M,eff}$ has the same trend of the molecular diffusivity as a function of pressure, while Knudsen diffusivity (Eq. (12)) is independent on pressure.

$$\mathfrak{D}_{K,eff} = \mathfrak{D}_K \frac{\theta}{\tau} = 9700 \times \frac{2}{SSA \, \rho_b} \sqrt{\frac{T}{M}} \frac{\theta^2}{\tau^2}; \tag{12}$$

In Eq. (12) T is the absolute temperature, M is the molecular weight (very close to air one in the present case), SSA the total specific surface area (1.4×10^6 cm^2 s^{-1} in the present case), ρ_b the catalyst density (1.3 g cm^{-3} in the present case).

As a consequence the predominance of Knudsen or ordinary diffusion depends not only on pore size but also on the D/D_K ratio, which in turn depends on pressure. The diffusion flux for the Knudsen mechanism increases by increasing the pressure and then becomes constant when ordinary diffusivity becomes the predominant mechanism [45]. Accordingly the Weisz–Prater criterion will be applied for the minimum pressure (i.e. the atmospheric one) and the highest temperatures for the different fuels, i.e. under conditions more influenced by internal mass transfer limitations. Table 4 summarizes the values of both Knudsen and ordinary $\mathfrak{D}_{eff}$ and Φ values.

The Knudsen diffusivity is lower by two orders of magnitude if compared to the ordinary one; as a consequence, effective diffusion is practically equal to the Knudsen one. The estimated Φ values for methane and hydrogen combustion are lower than 0.3

Table 4
Weisz modulus computed for different fuels.

CH$_4$			H$_2$			CO		
$\mathfrak{D}_{K,eff}$	$\mathfrak{D}_{M,eff}$	Φ	$\mathfrak{D}_{K,eff}$	$\mathfrak{D}_{M,eff}$	Φ	$\mathfrak{D}_{K,eff}$	$\mathfrak{D}_{M,eff}$	Φ
1.46	151	8×10^{-2}	1.46	548	1.3×10^{-1}	1.46	104	3.6×10^{-1}

$P = 1$ atm; $T = 800\,°C$; τ and θ respectively of 4 and 0.3. $S_g = 1.4 \times 10^6$ cm^2 s^{-1}, $\rho_b = 1.3$ g cm^{-3}, diffusivities are expressed in m^2 s^{-1} and are multiplied for 10^7, r_v (mol (s l)$^{-1}$) is calculated from data of Table 4 at 800 °C.
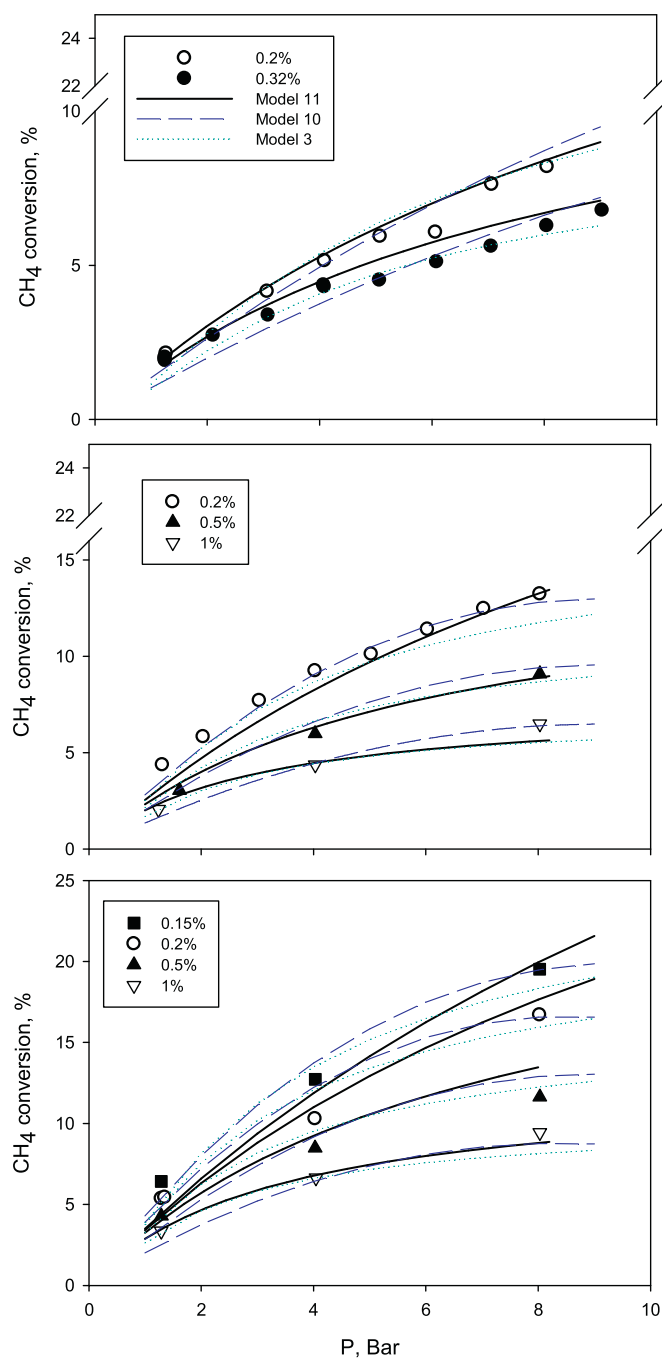
Fig. 3. CH_4 conversion as a function of pressure over LM20 platelet. (a) $T = 555\,°C$, total flow rate = 55 slph; (b) $T = 595\,°C$; total flow rate = 80 slph; (c) $T = 620\,°C$; total flow rate = 80 slph. Symbols: experimental data; black solid lines: simulated values with model 11; blue dashed lines simulated value with model 10; green dotted lines: simulated value with model 3. (For interpretation of the references to color in this figure legend, the reader is referred to the web version of this article.)

even at $800\,°C$. As regards CO combustion, the Φ value calculated at $800\,°C$ is slightly higher than 0.3 suggesting that the combustion tests could be carried out below $800\,°C$.

4. Results

As modus operandi, we first selected for each fuel the kinetic model by deriving the global parameter and comparing the fitting results. We then choose the best kinetic model and we then
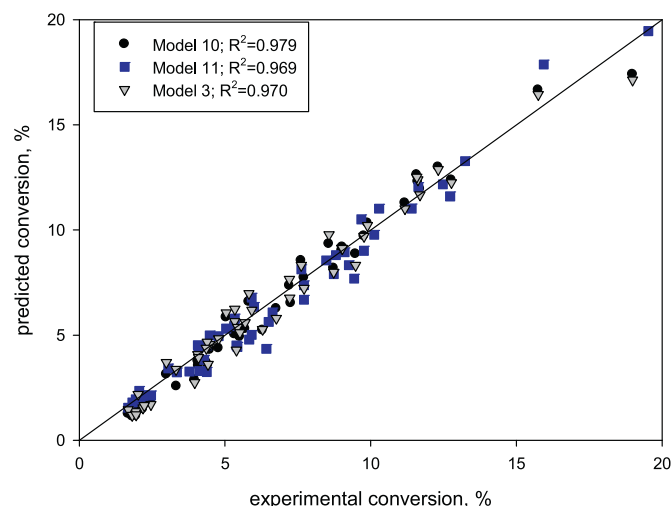

Fig. 4. Predicted versus experimental conversion values for CH_4 combustion.

identified the pre-exponential factor, the activation energy and the adsorption/desorption heats.

4.1. Methane combustion

Fig. 3 shows methane conversion as a function of pressure at different values of the inlet methane concentration $y^{\circ}_{CH_4}$ (O_2 content equal to 8.5%) at $555\,°C$ (Fig. 3a), $595\,°C$ (Fig. 3b) and $620\,°C$ (Fig. 3c).

CH_4 conversion increases by increasing pressure but decreases by increasing methane concentration. It is also worth noting that the higher is the pressure, the higher is the sensitivity of CH_4 conversion to inlet CH_4 concentration. This result suggests that the pressure has an inhibiting effect on methane combustion. An inhibiting effect of pressure on methane combustion was found also for noble metal catalysts and in particular for Pt-based catalyst by Reinke et al. [22] and Snow et al. [32].

4.1.1. Model discrimination

To identify the best kinetic model we first performed the screening of different kinetic models available in the literature [46,47]. The tested kinetic models given in Table 5 are the Eley–Rideal models (1 and 2), the Langmuir–Hinshelwood models (3–8) and the Mars–van Krevelen models (9, 10). We then estimated the kinetic parameters at each temperature, given in Table 5.

From the obtained results we rejected models 1, 2, 4, 5, 6, 8 and 9 because of their poor statistical fitting (1, 2, 6 and 8) or because they give negative values of the parameters (4, 5 and 9).

It is worth noting that the oxygen adsorption constant (K_o) of model 3 increases by increasing the temperature (i.e. the heat of adsorption is positive). Such behavior could be related to the double nature of oxygen species on the perovskite surface, α- and β-oxygen. α-Oxygen (O_{ads}) is active toward hydrocarbon oxidation at low temperature, while β-oxygen (O_{lat}) is active at high temperature and, under certain circumstances, makes the reaction rate independent of the oxygen partial pressure [8,11,48,49]. The two species are related by the relative velocity of dissociative adsorption and oxygen transfer into the lattice structure.

$$\tfrac{1}{2}O_2 \Leftrightarrow O_{ads} \Leftrightarrow O_{lat}$$
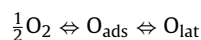
At high temperature, it is expected that only β-oxygen is available (temperature promotes the diffusion of β-oxygen from the lattice to the surface) and that the reaction order of oxygen approaches zero, while at low temperature oxygen partial pressure effect on kinetics must be taken into account and provides a reaction order with respect to oxygen equal to 0.5 ([50–52], as examples). As a

Table 5
Results of fitting experimental kinetic data of CH_4 combustion on LM20 to several rate models.

	Rate expression	$T = 555\,°C$	$T = 595\,°C$	$T = 620\,°C$
1	$r = \frac{k_s K_m P_m P_o}{1 + K_m P_m}$	$k_s = (8 \pm 8.3) \times 10^{-6}$ $K_m = 94 \pm 214$ Mrss = 4.7 $F = 6.22$ $R^2 = 0.24$	$k_s = (1.1 \pm 1) \times 10^{-5}$ $K_m = 80 \pm 125$ Mrss = 7.4 $F = 8.64$ $R^2 = 0.38$	$k_s = (4.2 \pm 5) \times 10^{-5}$ $K_m = 64 \pm 140$ Mrss = 19 $F = 3.0$ $R^2 = 0.2$
2	$r = \frac{k_s K_o P_m P_o}{1 + K_o P_o}$		The model is unable to fit the data	
3	$r = \frac{k_s K_o K_m P_m P_o}{(1 + K_m P_m + K_o P_o)^2}$	$k_s = (3 \pm 0.07) \times 10^{-5}$ $K_m = 79.7 \pm 34.1$ $K_o = 2.51 \pm 0.85$ Mrss = 0.43 $F = 139$ $R^2 = 0.94$	$k_s = (1.0 \pm 0.3) \times 10^{-4}$ $K_m = 46 \pm 16$ $K_o = 6.0 \pm 1.8$ Mrss = 0.25 $F = 237$ $R^2 = 0.97$	$k_s = (1.5 \pm 0.3) \times 10^{-4}$ $K_m = 44 \pm 18$ $K_o = 6.9 \pm 2$ Mrss = 1 $F = 140$ $R^2 = 0.96$
4	$r = \frac{k_m (P_m - P_p P_s / K P_o)}{(1 + K_o P_o + K_m P_p P_s / K P_o)}$		K_o and K show negative values	
5	$r = \frac{k_m (P_m - P_p P_s / K P_o)}{(1 + \sqrt{K_o P_o} + K_m P_p P_s / K P_o)}$		K shows negative value	
6	$r = \frac{k_m (P_m - P_p P_s / K P_o)}{(1 + K_m P_p P_s / K P_o)}$	$k_m = (4.8 \pm 0.5) \times 10^{-4}$ $K_m = (1.1 \pm 1000) \times 10^4$ $K = (1.6 \pm 1000) \times 10^{-2}$ Mrss = 0.45 $F = 215$ $R^2 = 0.96$	$k_m = (9.4 \pm 1.8) \times 10^{-4}$ $K_m = 434 \pm 3000$ $K = (4.4 \pm 33) \times 10^{-3}$ Mrss = 0.58 $F = 140$ $R^2 = 0.96$	$k_m = (1.4 \pm 0.8) \times 10^{-3}$ $K_m = 42.7 \pm 4000$ $K = (2.1 \pm 28) \cdot 10^{-3}$ Mrss = 0.85 $F = 176$ $R^2 = 0.97$
7	$r = \frac{k_o (P_o - P_p P_s / K P_m)}{(1 + K_m P_m + K_o P_p P_s / K P_m)}$		The model is unable to fit the data	
8	$r = \frac{k_o (P_o - P_p P_s / K P_m)}{(1 + K_m P_m + \sqrt{K_o P_p P_s / K P_m})^2}$		The model is unable to fit the data	
9	$r = \frac{k_1 k_2 P_m P_o}{k_1 P_o + 2 k_2 P_m + k_1 k_2 / k_3 P_m P_o}$		k_3 shows a negative value	
10	$r = \frac{k_1 k_2 P_m P_o}{k_1 P_o + 2 k_2 P_m} \left(1 - \frac{k_1}{k_1^*} P_o\right)$	$k_1 = (3.1 \pm 0.8) \times 10^{-5}$ $k_2 = (6.7 \pm 2.7) \times 10^{-4}$ $k_1^* = (1.1 \pm 0.76) \times 10^{-4}$ Mrss = 0.36 $F = 165$ $R^2 = 0.95$	$k_1 = (1.8 \pm 0.5) \times 10^{-4}$ $k_2 = (1.5 \pm 0.2) \times 10^{-3}$ $k_1^* = (2.8 \pm 0.9) \times 10^{-4}$ Mrss = 0.3 $F = 301$ $R^2 = 0.98$	$k_1 = (2.9 \pm 1) \times 10^{-4}$ $k_2 = (2.0 \pm 0.4) \times 10^{-3}$ $k_1^* = (4.1 \pm 1) \times 10^{-4}$ Mrss = 0.95 $F = 158$ $R^2 = 0.96$
11	$r = \frac{k P_m}{1 + k_m P_m}$	$k = (4.0 \pm 0.7) \times 10^{-4}$ $K = 47.2 \pm 18$ Mrss = 0.49 $F = 493$ $R^2 = 0.96$	$k = (1.1 \pm 0.5) \times 10^{-3}$ $K = 42.9 \pm 7$ Mrss = 0.67 $F = 321$ $R^2 = 0.94$	$k = (1.3 \pm 0.3) \times 10^{-3}$ $K = 36.4 \pm 10.7$ Mrss = 1.6 $F = 167$ $R^2 = 0.94$

Mrss values are multiplied per 10^4.

Table 6
Kinetic parameters of the best models estimated according to Eqs. (3) and (4).

|	
Model 3 $r = \frac{k_{SR} K_o K_m P_m P_o}{(1 + K_m P_m + K_o P_o)^2}$	$K_{sr}^\circ = (7.40 \pm 0.3) \times 10^{-5}$ $E_a = 36.6 \pm 2.0\ \text{kcal mol}^{-1}$ $K_m^\circ = 54.7 \pm 4.6\ \text{bar}^{-1}$ $\Delta H_m = -13.8 \pm 4.6\ \text{kcal mol}^{-1}$ $K_o^\circ = 4.7 \pm 0.53\ \text{bar}^{-1}$ $\Delta H_o = 23.5 \pm 6.1\ \text{kcal mol}^{-1}$
Model 10 $r = \frac{k_1 k_2 P_m P_o}{k_1 P_o + 2 k_2 P_m} \left(1 - \frac{k_1}{k_1^*} P_o\right)$	$k_1^\circ = (1.18 \pm 0.2) \times 10^{-4}\ \text{mol (g s bar)}^{-1}$ $E_{a1} = 52.3 \pm 9.1\ \text{kcal mol}^{-1}$ $k_2^\circ = (1.26 \pm 0.06) \times 10^{-3}\ \text{mol (g s bar)}^{-1}$ $E_{a2} = 25.1 \pm 2.5\ \text{kcal mol}^{-1}$ $k_1^{*\circ} = (2.31 \pm 0.1) \times 10^{-4}\ \text{mol (g s bar)}^{-1}$ $E_{a1^*} = 30.5 \pm 2.1\ \text{kcal mol}^{-1}$
Model 11 $r = \frac{k P_m}{1 + K P_m}$	$k^\circ = 8.3 \pm 1.0 \times 10^{-4}\ \text{mol (g s bar)}^{-1}$ $E_a = 27.6 \pm 6.74\ \text{kcal mol}^{-1}$ $K^\circ = 41.9 \pm 1.35\ \text{bar}^{-1}$ $\Delta H_m = -5.58 \pm 1.75\ \text{kcal mol}^{-1}$
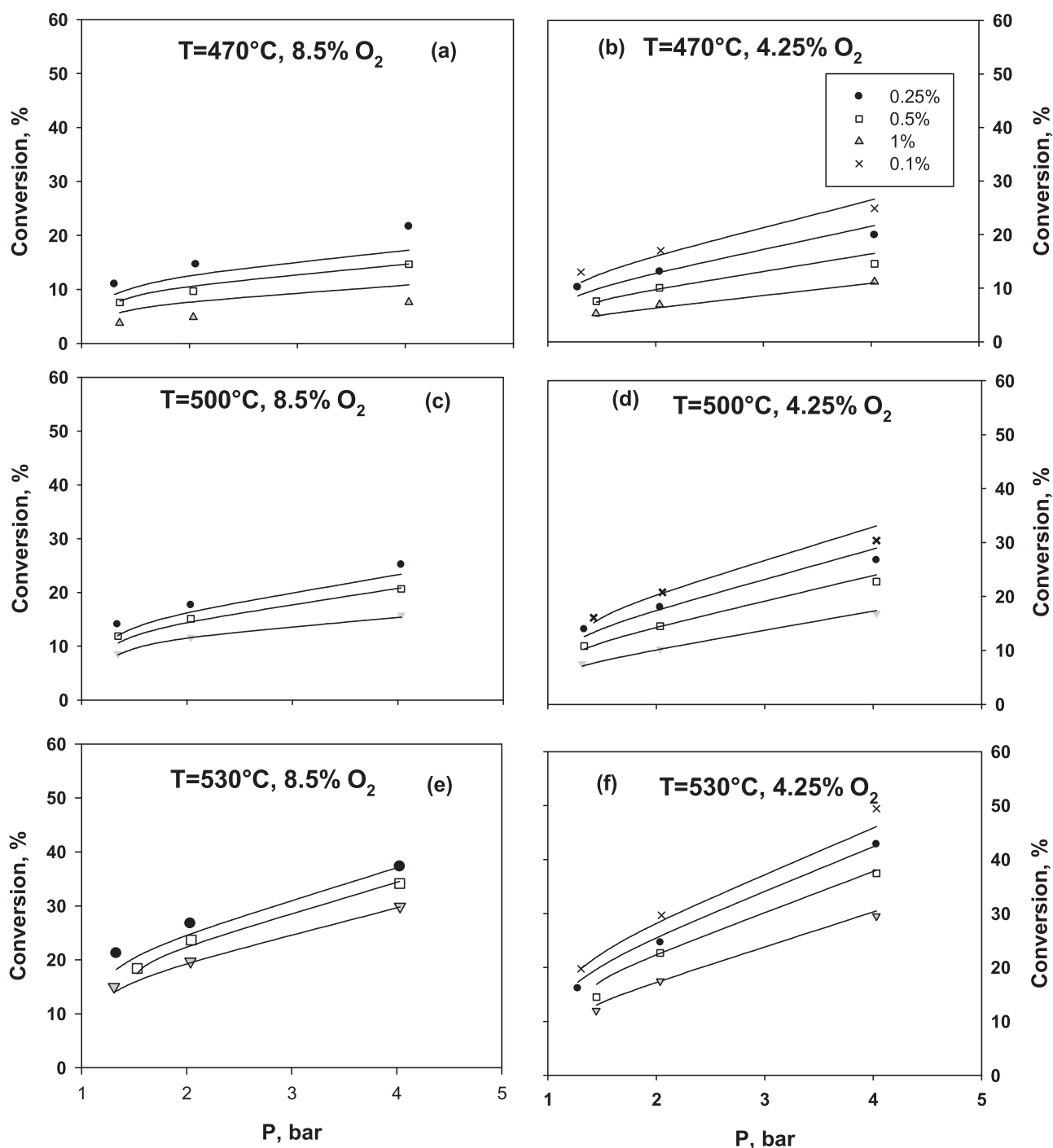
Fig. 5. CO conversion as a function of the total pressure and parametric in the initial CO molar fraction y_{CO}° on LM20 platelet. (a), (c) and (e) 8.5% O_2 temperature respectively of 470 °C, 500 °C and 530 °C. (b), (d) and (f): 4.25%O_2 temperature respectively of 470 °C, 500 °C and 530 °C. Symbols: experimental data; lines: predicted conversion according to model 17.

consequence, K_o in model 3 could be seen as a combination of a typical adsorption constant (decreasing by increasing the temperature) and an equilibrium constant of a spillover process (increasing by increasing the temperature), with the latter predominant in the investigated temperature range.

Model 10 was also tested by Auer et al. [46] over a La–Ce–Co perovskite catalyst. This model is based on the assumption that

the reaction rate of the oxygen adsorption (k_1 as kinetic constant), oxygen dissociation (k_1^* as kinetic constant) and catalyst reduction by the fuel (k_2 as kinetic constant) are comparable [46].

Model 11 shows a quite good fitting of the experimental data. It may be derived from model 3 by assuming that the number of oxidized sites is fairly constant, thus implying that the re-oxidation rate is very fast.

4.1.2. Kinetic model identification

In Table 6, the estimated values of the kinetic parameters for the best models (3, 10 and 11) are given.

The activation energies of model 10 are in line or slightly higher than those reported by Auer et al. [46] except for that of k_1. In any case, activation energies of surface reaction steps in models 3, 10 and 11 are comparable to those reported in the literature for similar perovskite-based catalysts [8,18,52].

In Fig. 4 the model values are plotted as a function of the experimental ones as obtained by using the models of Table 6 together with the regression factors which are higher than 0.96 for all models.

4.2. Carbon monoxide combustion

Kinetic catalytic tests of CO combustion have been carried out in the temperature range 470–530 °C and by varying the $y^\circ_{O_2}$ and y°_{CO} in the range of 0.25–8.5% and 0.1–1%, respectively. In Fig. 5, CO conversion as a function of the total pressure is reported for two O_2 initial fraction (4.5 and 8.5%) at the three temperatures investigated. In all the tests the total flow rate is constant and equal to 75 slph.

CO conversion decreases by increasing fuel concentration at fixed pressure and $y^\circ_{O_2}$. Changing oxygen concentration results in a slight but not negligible variation of the CO conversion, suggesting that variation of oxygen coverage due to steps including oxygen adsorption and surface transfer cannot be neglected.

4.2.1. Model discrimination

The results of some selected and most remarkable models tested for the carbon monoxide combustion are resumed in Table 7 together with the relative parameters estimations and statistical parameters.

The models are the same as used for methane with some differences due to stoichiometric factors except of model 15 which was proposed in the literature for CO combustion over noble metal catalysts [35,53,54].

The normality test on the residual distribution is failed for models 12 and 15 (i.e. residuals distributions are not Gaussian), suggesting the inadequacy of these models.

The other models show very good data fitting, models 16 and 17 exhibiting the best data fitting as demonstrated by their Mrss value. It is worth saying that model 17 corresponds to model 10 for methane combustion. As a consequence, this model shows good data fitting for both CH_4 and CO combustion.

4.2.2. Kinetic model identification

In Table 8 the kinetic parameters for the best models (13, 15, 16 and 17) are given. From the data reported in Table 8, it appears that in model 13 the CO and O_2 heats of adsorption are badly estimated showing standard errors of the same order of the estimated parameter.

A similar problem was encountered in the k_1 estimation in model 16.

On the other hand, kinetic parameters of models 14 and 17 are well estimated. Concerning the positive estimated value of O_2 heat of adsorption in model 14 similar considerations about the double nature of oxygen species present on the catalyst can be done (see Section 4.1.1).

In Fig. 6 the model values of the CO conversion are plotted as a function of the experimental data.

From all these data, it results that the best model is a Mars–van Krevelen mechanism (model 17). This result is in agreement with Ramesh et al. [55] who derived a Mars–van Krevelen kinetic equation for CO oxidation over manganese oxide catalysts.
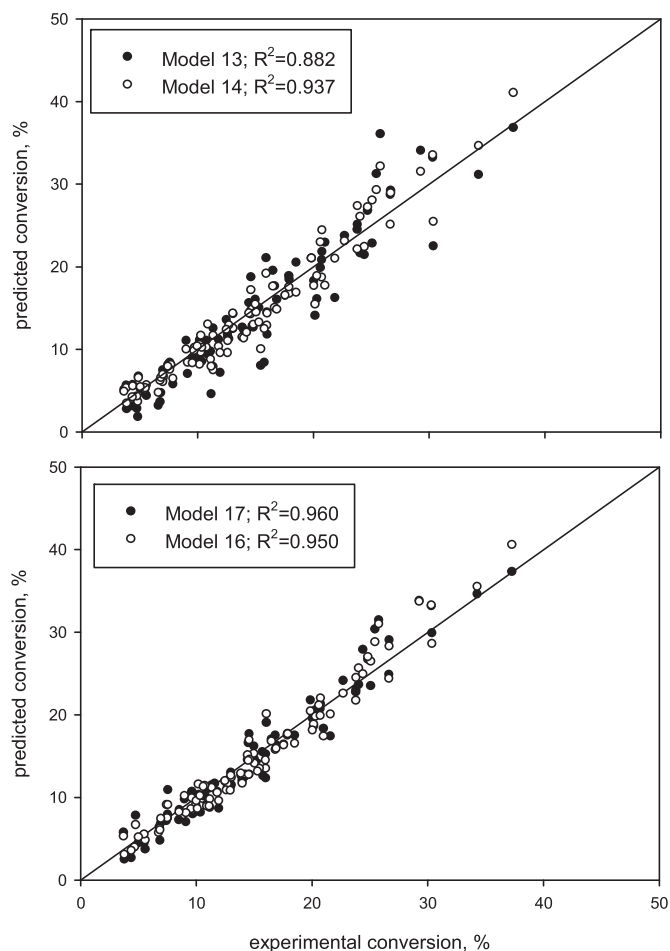

Fig. 6. Predicted versus experimental conversion values for CO combustion.

4.3. Hydrogen combustion

Kinetic tests of H_2 combustion have been carried out in the temperature range 470–530 °C and by varying the $y^\circ_{O_2}$ and $y^\circ_{H_2}$ in the range of 4–8.5% and 0.25–1%, respectively.

In Fig. 7 H_2 conversion as a function of the total pressure is reported at three initial molar fractions and fixed O_2 content (8.5 vol.%). In all the tests the total flow rate is kept constant and equal to 100 slph. From Fig. 7 it appears that H_2 consumption rate is first order with respect to H_2 partial pressure.

The effect of oxygen concentration on H_2 conversion has been performed at 8.5% and 4% O_2. Results at 500 °C and H_2 content equal to 0.95% are shown in Fig. 8. As shown in Fig. 8, an increase of the oxygen concentration negatively affects the hydrogen conversion.

4.3.1. Model discrimination and identification

In the development of suitable kinetic models to test we started from the reaction mechanism of hydrogen combustion over metals proposed by Hellsig et al. [56]. If the sequential hydrogen addition step (k as kinetic constant; K_{eq} is the equilibrium constant of the reaction $H\sigma + O\sigma \leftrightarrow OH\sigma + \sigma$) is assumed as the controlling step, the following rate expression is derived (Eq. (13)):

$$r = \frac{kK_h P_h \sqrt{K_o P_o}}{\left(1 + \sqrt{K_h P_h} + \sqrt{K_o P_o} + K_{eq}\sqrt{K_h P_h}\sqrt{K_o P_o}\right)^2} \tag{13}$$

Table 7
Results of fitting experimental for CO combustion data with several rate models.

	Model	$T = 470\,^\circ C$	$T = 500\,^\circ C$	$T = 530\,^\circ C$
12	$r = \frac{k \cdot P_c \cdot P_o}{1 + K_c \cdot P_c}$	$k = (7.9 \pm 2.8) \times 10^{-5}$ $K_c = (1.4 \pm 3.4) \times 10^3$ Mrss = 29 $F = 10$ $R^2 = -0.1$	$k = (1.4 \pm 0.94) \times 10^{-4}$ $K_c = 260 \pm 423$ Mrss = 60 $F = 1.3$ $R^2 = 0.12$	$k = (5.1 \pm 5.9) \times 10^{-4}$ $K_c = 62.5 \pm 124$ Mrss = 46 $F = 4.3$ $R^2 = 0.12$
13	$r = \frac{k \cdot K_c \cdot P_c \cdot K_o \cdot P_o}{(1 + K_c \cdot P_c + K_o \cdot P_o)^2}$	$k = (1.3 \pm 0.4) \times 10^{-4}$ $K_c = 102.3 \pm 19.8$ $K_o = 13.7 \pm 1.6$ Mrss = 4.6 $F = 94.7$ $R^2 = 0.83$	$k = (3.0 \pm 0.6) \times 10^{-4}$ $K_c = 47.9 \pm 12.9$ $K_o = 10.6 \pm 2.3$ Mrss = 0.9 $F = 280$ $R^2 = 0.98$	$k = (4.2 \pm 0.9) \times 10^{-4}$ $K_c = 71.2 \pm 26.0$ $K_o = 13.1 \pm 2.7$ Mrss = 1.8 $F = 317$ $R^2 = 0.67$
14	$r = \frac{k \cdot K_c \cdot P_c \cdot \sqrt{K_o \cdot P_o}}{(1 + K_c \cdot P_c + \sqrt{K_o \cdot P_o})^2}$	$k = (1.9 \pm 0.4) \times 10^{-4}$ $K_c = 62.5 \pm 14.2$ $K_o = 3.7 \pm 3$ Mrss = 2.4 $F = 206$ $R^2 = 0.91$	$k = (3.9 \pm 0.6) \times 10^{-4}$ $K_c = 34.7 \pm 28.9$ $K_o = 3.81 \pm 0.9$ Mrss = 1.6 $F = 74$ $R^2 = 0.90$	$k = (7.0 \pm 1.6) \times 10^{-4}$ $K_c = 29.7 \pm 8.5$ $K_o = 4.0 \pm 2.0$ Mrss = 8.3 $F = 85$ $R^2 = 0.84$
15	$r = \frac{k \cdot K_c \cdot P_c \cdot \sqrt{P_o}}{(1 + K_c \cdot P_c)^2}$	$k = (1.8 \pm 0.3) \times 10^{-4}$ $K_c = 55.3 \pm 17.5$ Mrss = 8.4 $F = 85.8$ $R^2 = 0.68$	$k = (3.2 \pm 1.3) \times 10^{-4}$ $K_c = 28.4 \pm 18.3$ Mrss = 17 $F = 19.2$ $R^2 = 0.66$	$k = (6.5 \pm 2.1) \times 10^{-4}$ $K_c = 25.9 \pm 14.1$ Mrss = 46 $F = 4.3$ $R^2 = 0.11$
16	$r = \frac{k_1 k_2 P_c P_o}{k_1 P_o + 0.5 k_2 P_c + (k_1 k_2 / k_3) P_c P_o}$	$k_1 = (3.3 \pm 0.9) \times 10^{-4}$ $k_2 = (3.1 \pm 0.4) \times 10^{-3}$ $k_3 = (4.8 \pm 1.1) \times 10^{-5}$ Mrss = 1.9 $F = 260$ $R^2 = 0.93$	$k_1 = (3.0 \pm 11) \times 10^{-3}$ $k_2 = (3.5 \pm 0.3) \times 10^{-3}$ $k_3 = (7.7 \pm 2.5) \times 10^{-5}$ Mrss = 2.3 $F = 148$ $R^2 = 0.95$	$k_1 = (9.8 \pm 1.6) \times 10^{-4}$ $k_2 = (5.1 \pm 0.7) \times 10^{-3}$ $k_3 = (2.2 \pm 1.3) \times 10^{-4}$ Mrss = 4.8 $F = 158$ $R^2 = 0.91$
17	$r = \frac{k_1 k_2 P_c P_o}{k_1 P_o + 0.5 k_2 P_c} \left(1 - \frac{k_1}{k_1^*} P_o\right)$	$k_1 = (1.8 \pm 0.3) \times 10^{-4}$ $k_2 = (3.6 \pm 0.7) \times 10^{-3}$ $k_1^* = (1.4 \pm 0.4) \times 10^{-4}$ Mrss = 3.7 $F = 110$ $R^2 = 0.87$	$k_1 = (3.2 \pm 0.7) \times 10^{-4}$ $k_2 = (4.2 \pm 0.5) \times 10^{-3}$ $k_1^* = (2.7 \pm 0.7) \times 10^{-4}$ Mrss = 1.8 $F = 183$ $R^2 = 0.96$	$k_1 = (6.8 \pm 1.2) \times 10^{-4}$ $k_2 = (5.8 \pm 1.1) \times 10^{-3}$ $k_1^* = (7.9 \pm 4) \times 10^{-4}$ Mrss = 5.7 $F = 131$ $R^2 = 0.89$

Table 8
Global parameters of the best models for the CO combustion estimated according to Eqs. (3) and (4).

|	
Model 13 $r = \frac{k \cdot K_c \cdot P_c \cdot K_o \cdot P_o}{(1 + K_c \cdot P_c + K_o \cdot P_o)^2}$	$k_{sr}^\circ = (2.54 \pm 0.29) \times 10^{-4}$ $E_a = 23.2 \pm 5.16\,\text{kcal mol}^{-1}$ $K_c^\circ = (7.04 \pm 1.9) \times 10^1\ \text{bar}^{-1}$ $\Delta H_c = -7.4 \pm 12\,\text{kcal mol}^{-1}$ $K_o^\circ = 12.4 \pm 1.36\,\text{bar}^{-1}$ $\Delta H_o = -1 \pm 5.3\,\text{kcal mol}^{-1}$
Model 14 $r = \frac{k \cdot K_c \cdot P_c \cdot \sqrt{K_o \cdot P_o}}{(1 + K_c \cdot P_c + \sqrt{K_o \cdot P_o})^2}$	$k_{sr}^\circ = (3.75 \pm 0.11) \times 10^{-4}\,\text{mol}\,(\text{g s bar})^{-1}$ $E_a = 25.7 \pm 4\,\text{kcal mol}^{-1}$ $K_c^\circ = 40.1 \pm 3.83\,\text{bar}^{-1}$ $\Delta H_c = -14.75 \pm 4.6\,\text{kcal mol}^{-1}$ $K_o^\circ = 3.83 \pm 0.02\,\text{bar}^{-1}$ $\Delta H_o = 1.53 \pm 0.25\,\text{kcal mol}^{-1}$
Model 16 $r = \frac{k_1 k_2 P_c P_o}{k_1 P_o + 0.5 k_2 P_c + (k_1 k_2 / k_3) P_c P_o}$	$k_1^\circ = (9.96 \pm 8.6) \times 10^{-4}\,\text{mol}\,(\text{g s bar})^{-1}$ $E_{a1} = 22.3 \pm 37.6\,\text{kcal mol}^{-1}$ $k_2^\circ = (3.81 \pm 0.25) \times 10^{-3}\,\text{mol}\,(\text{g s bar})^{-1}$ $E_{a2} = 9.73 \pm 3.1\,\text{kcal mol}^{-1}$ $k_3^\circ = (9.28 \pm 1.4) \times 10^{-5}\,\text{mol}\,(\text{g s bar})^{-1}$ $E_{a3} = 29.88 \pm 7.2\,\text{kcal mol}^{-1}$
Model 17 $r = \frac{k_1 k_2 P_c P_o}{k_1 P_o + 0.5 k_2 P_c} \left(1 - \frac{k_1}{k_1^*} P_o\right)$	$k_1^\circ = (3.39 \pm 0.18) \times 10^{-4}\,\text{mol}\,(\text{g s bar})^{-1}$ $E_{a1} = 26.1 \pm 2.6\,\text{kcal mol}^{-1}$ $k_2^\circ = (4.44 \pm 0.19) \times 10^{-3}\,\text{mol}\,(\text{g s bar})^{-1}$ $E_{a2} = 9.34 \pm 2.6\,\text{kcal mol}^{-1}$ $k_1^{*\circ} = (3.10 \pm 0.35) \times 10^{-4}\,\text{mol}\,(\text{g s bar})^{-1}$ $E_{a1}^* = 33.94 \pm 5.50\,\text{kcal mol}^{-1}$
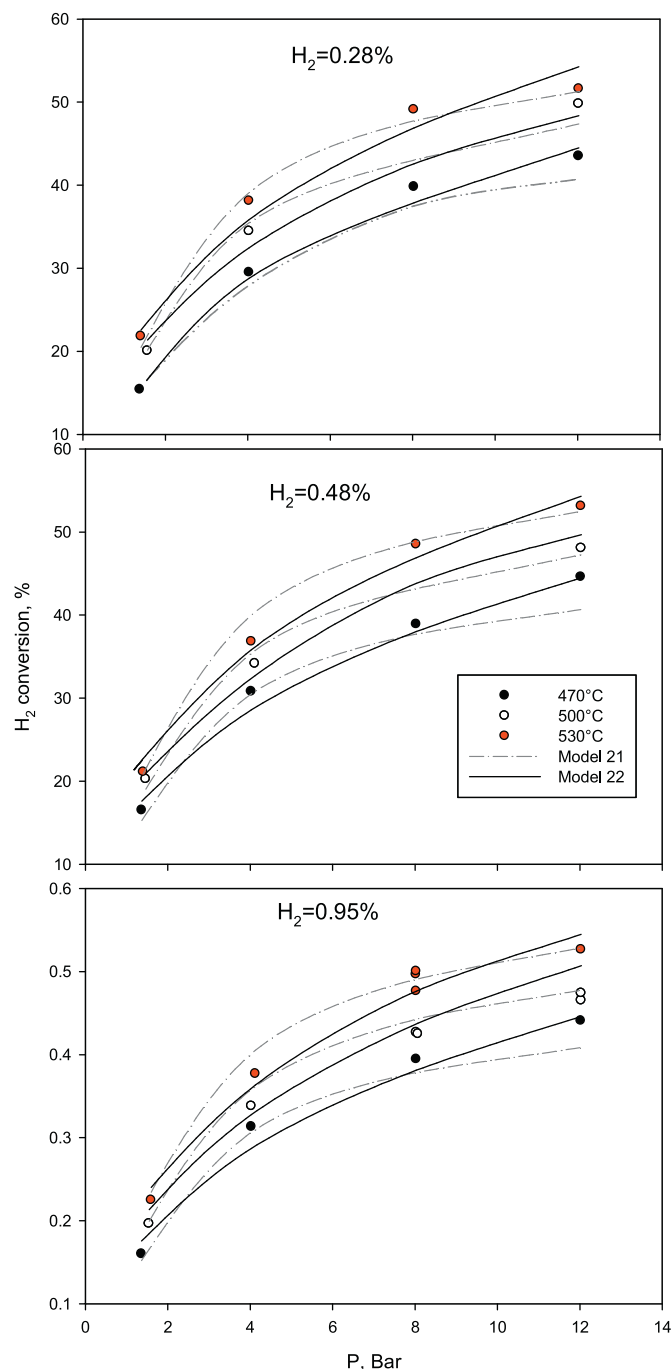
Fig. 7. H_2 conversion as a function of the total pressure and parametric in the temperature. $y_{H_2}^{\circ}$ (a) 0.28%; (b) 0.48% and (c) 0.95%. $O_2 = 8.5\%$. Total flow rate 100 slph. Symbols: experimental data; solid lines: predicted conversion according to model 22; dashed lines: predicted conversion according to model 21.

When $\sqrt{K_h P_h}$ and $K_{eq}\sqrt{K_h P_h}\sqrt{K_o P_o}$ are much lower than 1, Eq. (13) reduces to Eq. (14):

$$r = \frac{kP_h\sqrt{K_o P_o}}{\left(1 + \sqrt{K_o P_o}\right)^2} \tag{14}$$

which returns a linear dependence on hydrogen partial pressure according to the results shown in Fig. 7. Therefore, model 22 of Table 9 is equal to the expression reported in Eq. (14).
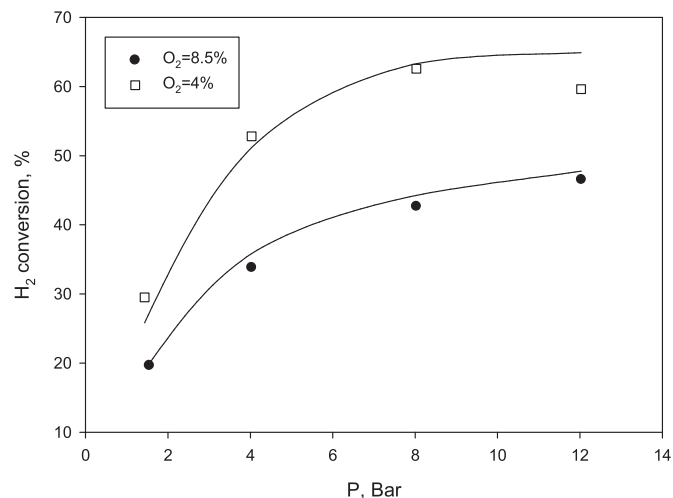

Fig. 8. H_2 conversion as a function of the total pressure at different $y_{O_2}^{\circ}$. $y_{H_2}^{\circ}$ 0.95%; $T = 500\,^{\circ}C$; total flow rate: 100 slph.

If the OH disproportionation reaction (k' as kinetic constant) is assumed as the limiting step, the following expression is found:

$$r = \frac{k' \cdot (K_{eq})^2 K_h P_h K_o P_o}{\left(1 + \sqrt{K_h P_h} + \sqrt{K_o P_o} + K_{eq}\sqrt{K_h P_h}\sqrt{K_o P_o}\right)^2} \tag{15}$$

When $\sqrt{K_h P_h}$ and $K_{eq}\sqrt{K_h P_h}\sqrt{K_o P_o}$ are much lower than 1, once again a linear dependence on P_h was found and Eq. (15) reduces to Eq. (16), reported as model 20 of Table 9.

$$r = \frac{kP_h K_o P_o}{\left(1 + \sqrt{K_o P_o}\right)^2} \tag{16}$$

Table 9 reports some of the kinetic expressions chosen for the regression of H_2 combustion.

We also tested Eley–Rideal kinetic models derived assuming that the limiting step is the surface reaction between gas phase hydrogen and adsorbed molecular oxygen (model 18) or dissociative adsorbed oxygen (model 19).

Model 21 is a Langmuir–Hinshelwood model mechanism in which the limiting step is the surface reaction between adsorbed H_2 and adsorbed O_2.

In Table 9 the values of the kinetic parameters obtained by the fitting procedure are given for each model.

The results reported in Table 9 show that the Eley–Rideal type models are not able to fit the experimental data since the distribution of residuals is biased. Conversely, models 21 and 22 give very good data fitting as confirmed by the statistics reported in Table 9, by the model curves of Figs. 7 and 8 and by the parity plot (Fig. 9).

Model 21 gives a slightly better regression of the experimental data as it could be seen by comparing the F values, but the difference is marginal (see solid and dashed lines in Figs. 7 and 8). In this case, the estimated parameters are not affected by strong correlation while in model 22, a strong correlation affecting the four estimates and preventing discussion of their individual values is found.

The low value of the activation energy ($E_a = 6.5$ kcal mol^{-1}) suggests that the kinetic constant k is a combination of a proper kinetic constant and an equilibrium constant rather than the kinetic constant of an elemental step, which is confirmed when deriving Eqs. (14) and (16).

In conclusion, kinetic expression of the model 21 is able to regress the data in the studied range of temperature and reactant concentration, but cannot give full information on the actual reaction mechanism. Moreover, the four parameters are well estimated. On the other hand, model 22 appears more realistic from a

Table 9
Global parameters of the best models for the H_2 combustion estimated according to Eqs. (3) and (4).

	Model		
18	$r = \frac{kP_h K_o P_o}{1 + K_o P_o}$	$F = 11$ $R^2 = 0.49$	$k^\circ = 3.1 \times 10^{-3}\ \mathrm{mol\,(g\,s\,bar)^{-1}}$ $E_a = 6.89\ \mathrm{kcal\,mol^{-1}}$ $K_{o_2}^\circ = 5.2 \times 10^7\ \mathrm{bar^{-1}}$ $\Delta H_{o_2} = 1.1\ \mathrm{kcal\,mol^{-1}}$
19	$r = \frac{kP_h \sqrt{K_o P_o}}{1 + \sqrt{K_o P_o}}$	$F = 2.8$ $R^2 = 0.19$	$k^\circ = (4.41 \pm 0.7) \times 10^{-3}\ \mathrm{mol\,(g\,s\,bar)^{-1}}$ $E_a = (5.69 \pm 2.1)\ \mathrm{kcal\,mol^{-1}}$ $K_o^\circ = 7.0 \pm 2.7\ \mathrm{bar^{-1}}$ $\Delta H_o = -(0.7 \pm 0.1)\ \mathrm{kcal\,mol^{-1}}$
20	$r = \frac{kP_h K_o P_o}{(1 + \sqrt{K_o P_o})^2}$	$F = 0.5$ $R^2 = 0.05$	$k^\circ = (5.0 \pm 0.8) \times 10^{-3}\ \mathrm{mol\,(g\,s\,bar)^{-1}}$ $E_a = 10.1 \pm 0.4\ \mathrm{kcal\,mol^{-1}}$ $K_o^\circ = 16.8 \pm 7\ \mathrm{bar^{-1}}$ $\Delta H_o = -9.8 \pm 0.3\ \mathrm{kcal\,mol^{-1}}$
21	$r = \frac{kP_h K_o P_o}{(1 + K_o P_o)^2}$	$F = 537;$ $R^2 = 0.978$	$k^\circ = (2.46 \pm 0.1) \times 10^{-2}\ \mathrm{mol\,(g\,s\,bar)^{-1}}$ $E_a = 6.49 \pm 0.2\ \mathrm{kcal\,mol^{-1}}$ $K_o^\circ = 8.35 \pm 0.8\ \mathrm{bar^{-1}}$ $\Delta H_o = -0.55 \pm 0.06\ \mathrm{kcal\,mol^{-1}}$
22	$r = \frac{kP_h \sqrt{K_o P_o}}{(1 + \sqrt{K_o P_o})^2}$	$F = 481$ $R^2 = 0.976$	$k^\circ = 2.49 \times 10^{-1}\ \mathrm{mol\,(g\,s\,bar)^{-1}}$ $E_a = 5.05\ \mathrm{kcal\,mol^{-1}}$ $K_o^\circ = 9.36\ \mathrm{bar^{-1}}$ $\Delta H_o = -1.0\ \mathrm{kcal\,mol^{-1}}$
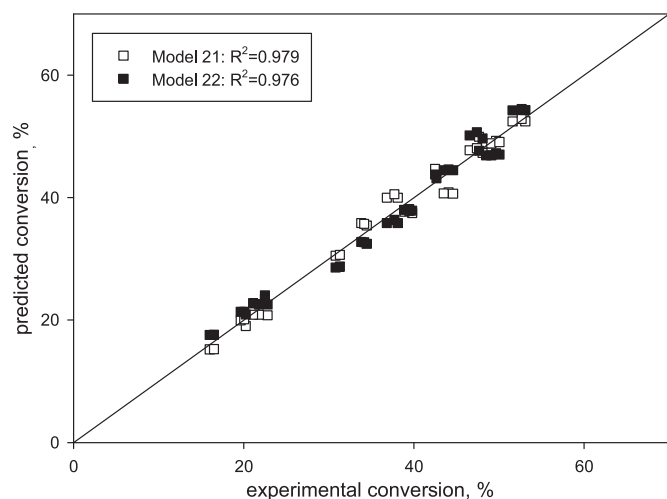
Fig. 9. Predicted versus experimental conversion values for H_2 combustion.

mechanistic point of view but it suffers from a strong correlation of estimates.

5. Conclusions

A kinetic study of the catalytic combustion of CH_4, H_2 and CO over a perovskite-based catalyst has been carried out to derive rate equations valid in a wide range of operating conditions of pressure, temperature, fuel concentration and equivalence ratio.

The experimental and numerical study has been performed in conditions relevant to ignition process which is surely controlled by the intrinsic kinetics.

A single Mars–van Krevelen mechanistic model was found to be able to well describe perovskite activity toward the oxidative activation of both CH_4 and CO, with differences due to oxygen availability mechanism. Even if the H_2 combustion has a linear dependence on hydrogen partial pressure, the Eley–Rideal type mechanisms fail to describe the H_2 oxidation kinetics; the best model has been derived from a Mars–van Krevelen mechanism with the assumption that the H_2 coverage of the surface is very low.

References

[1] J.H. Lee, D.L. Trimm, Fuel Processing Technology 42 (1995) 339–359.
[2] B. Major, B. Powers, Cost analysis of NO_x control alternatives for stationary gas turbine, Onsite Sycom [DOE Contract DE-FC02-97CHIO877], 1999.
[3] P. Dagaut, A. Nicolle, Proceedings of the Combustion Institute 30 (2005) 2631–2638.
[4] S.M. Walton, X. He, B.T. Zigler, M.S. Wooldridge, Proceedings of the Combustion Institute 31 (2007) 3147–3154.
[5] B. Towns, E.G. Slonik, J. Miller, R.W. Schefer, J.O. Keller, International Journal of Hydrogen Energy 32 (2007) 3093–3099.
[6] P.S. Barbato, G. Landi, G. Russo, Catalytic combustion of CH_4–H_2–CO mixtures at pressure up to 10 bar, Fuel Processing Technology (2012), http://dx.doi.org/10.1016/j.fuproc.2012.08.024, in press.
[7] M. Zwinkels, S. Jaras, P.G. Menon, T. Griffin, Catalysis Review: Science and Engineering 35 (1993) 319–358.
[8] T.V. Choudhary, S. Banerjee, V.R. Choudhary, Applied Catalysis A: General 234 (2002) 1–23.
[9] S. Colussi, A. Trovarelli, E. Vesselli, A. Baraldi, G. Comelli, G. Groppi, J. Llorca, Applied Catalysis A: General 390 (2010) 1–10.
[10] T. Seiyama, Catalysis Review: Science and Engineering 34 (1992) 281–301.
[11] H. Arai, T. Yamada, K. Eguchi, T. Seiyama, Applied Catalysis 26 (1986) 265–276.
[12] G. Saracco, F. Geobaldo, G. Baldi, Applied Catalysis B: Environmental 20 (1999) 277–288.
[13] S. Cimino, L. Lisi, R. Pirone, G. Russo, M. Turco, Catalysis Today 59 (2000) 19–31.
[14] P.E. Marti, M. Maciejewski, A. Baiker, Applied Catalysis B 4 (1994) 225–235.
[15] F. Cifà, P. Dinka, P. Viparelli, S. Lancione, G. Benedetti, P.L. Villa, M. Viviani, P. Nanni, Applied Catalysis B: Environmental 46 (2003) 463–471.
[16] L. Giebeler, D. Kiebling, G. Wendt, Chemical Engineering and Technology 30 (7) (2007) 889–894.
[17] M. Uenishi, M. Tanigushi, H. Tanaka, M. Rimura, Y. Nishihata, J. Mizuki, T. Kobayashi, Applied Catalysis B: Environmental 57 (2005) 267–273.
[18] B. Kucharczyk, W. Tylus, Catalysis Today 90 (2004) 121–126.
[19] A. Scarpa, P.S. Barbato, G. Landi, R. Pirone, G. Russo, Chemical Engineering Journal 154 (1–3) (2009) 315–324.
[20] R. Carroni, T. Griffin, J. Mantzaras, M. Reinke, Catalysis Today 83 (2003) 157–170.
[21] P.S. Barbato, A. Di Benedetto, V. Di Sarli, G. Landi, R. Pirone, Industrial and Engineering Chemical Research 51 (22) (2012) 7547–7558.
[22] A. Di Benedetto, G. Landi, V. Di Sarli, P.S. Barbato, R. Pirone, G. Russo, Catalysis Today 197 (1) (2012) 206–213.
[23] M. Reinke, J. Mantzaras, R. Schaeren, R. Bombach, A. Inauen, S. Schenker, Combustion and Flame 136 (2004) 217–240.
[24] K. Persson, A. Ersson, A. Manrique Carrera, J. Jayasuriya, R. Fakhrai, T. Fransson, S. Jaras, Catalysis Today 100 (2005) 479–483.

[25] M. Reinke, J. Mantzaras, R. Bombach, S. Schenker, A. Inaunen, Combustion and Flame 141 (2005) 448–468.
[26] J.C.G. Andrae, D. Johansson, M. Bursell, R. Fakhrai, J. Jayasuriya, A. Manrique Carrera, Applied Catalysis A: General 293 (2005) 129–136.
[27] K. Persson, L.D. Pfefferle, W. Schwartz, A. Ersson, S.G. Jaras, Applied Catalysis B: Environmental 74 (2007) 242–250.
[28] S.T. Kolaczkowski, S. Serbetcioglu, Applied Catalysis A: General 38 (2) (1996) 199–214.
[29] O. Deutschmann, L.I. Maier, U. Riedel, A.H. Stroemman, R.W. Dibble, Catalysis Today 59 (2000) 141–150.
[30] O. Deutschmann, R. Schmidt, F. Behrendt, J. Warnatz, Proceedings of the Combustion Institute 26 (1996) 1747–1754.
[31] Y.K. Park, P. Aghalayam, D.G. Vlachos, Journal of Physical Chemistry A 103 (1999) 8101–8107.
[32] J. Mantzara, T. Lieuwen, V. Yang, R. Yetter (Eds.), Synthesis Gas Combustion: Fundamentals and Applications, CRC Press-Taylor & Francis Group, New York, 2009, pp. 223–260.
[33] G.C. Snow, W.V. Krill, E.K. Chu, R.K. Kendall, Mechanisms and Kinetics in Catalytic Combustion, Report No. EPA-600/9-84-002, 1984, p. 105.
[34] J.G. McCarty, Catalysis Today 26 (1995) 283–293.
[35] G. Groppi, W. Ibashi, E. Tronconi, P. Forzatti, Chemical Engineering Journal 82 (2001) 57–71.
[36] G. Groppi, Catalysis Today 77 (2003) 335–346.
[37] A. Ersson, H. Kusar, R. Carroni, T. Griffin, S. Jaras, Catalysis Today 83 (1–4) (2003) 265–277.
[38] H. Arai, M. Machida, Applied Catalysis A: General 138 (1996) 161–176.
[39] http://www.cotronics.com/vo/cotr/pdf/700ins.pdf
[40] http://www.mathworks.it/help/toolbox/stats/nlinfit.html
[41] O. Levenspiel, Chemical Reaction Engineering, 2nd edn, John Wiley, New York, 1972.
[42] A. Pethö, R.D. Noble, Residence Time Distribution Theory in Chemical Engineering, Verlag Chemie, 1982.
[43] R.H. Perry, D.W. Green, Perry's Chemical Engineering Handbook, 7th edn, McGraw-Hill, New York, 1997.
[44] A. Beretta, G. Groppi, M. Lualdi, I. Tavazzi, P. Forzatti, Industrial and Engineering Chemical Research 48 (2009) 3825–3836.
[45] C.N. Satterfield, T.K. Sherwood, The Role of Diffusion in Catalysis, Addison-Wesley Pub. Co., 1963.
[46] R. Auer, L. Warnier, F.C. Thyrion, Studies in Surface Science and Catalysis 133 (2001) 599–604.
[47] P. Hurtado, S. Ordóñez, H. Sastre, F.V. Diez, Applied Catalysis B: Environmental 51 (2004) 229–238.
[48] A.K. Ladavos, P.J. Pomonis, Journal of the Chemical Society, Faraday Transactions 88 (1992) 2557–2562.
[49] Z.-B. Chen, T.-R. Ling, M.-D. Lee, Reaction Kinetics and Catalysis Letters 62 (1997) 185–190.
[50] D. Klvana, J. Vaillancourt, J. Kirchnerova, J. Chaouki, Applied Catalysis A 109 (1994) 181–193.
[51] C. Batiot-Dupeyrat, F. Martinez-Ortega, M. Ganne, J.M. Tatibouët, Applied Catalysis A: General 206 (2001) 205–215.
[52] G. Saracco, G. Scibilia, A. Iannibello, G. Baldi, Applied Catalysis B 8 (1996) 229–244.
[53] S.E. Voltz, C.R. Morgan, B.A. Liederman, Industrial and Engineering Chemistry: Process Design and Development 12 (1973) 294–301.
[54] C. Dubien, D. Schweich, G. Mabilon, B. Martin, M. Prigent, Chemical Engineering Science 53 (1998) 471–481.
[55] K. Ramesh, L. Chen, F. Chen, Y. Liu, Z. Wang, Y. Han, Catalysis Today 131 (2008) 477–482.
[56] B. Hellsing, B. Kasemo, V.P. Zhdanov, Journal of Catalysis 132 (1991) 210–228.